Progress In Electromagnetics Research C, Vol. 116, 37–49, 2021

Eight Shape Electromagnetic Band Gap Structure for Bandwidth Improvement of Wearable Antenna

Vidya R. Keshwani[1], Pramod P. Bhavarthe[2], and Surendra S. Rathod[1, *]

Abstract—In this paper, a rectangular eight shaped Electromagnetic Band Gap (EBG) structure at 5.8 GHz Industrial, Scientific and Medical (ISM) band for wearable application is proposed with intent to improve the impedance bandwidth of antenna. The unit cell of an EBG structure is formed using eight shape on outer ring with inner square patches. The simulation of the eight shape EBG unit cell is carried out using eigen mode solution of Ansys High Frequency Structure Simulator (HFSS). Simulated results are validated by experimental results. The application of proposed EBG for an inverse E-shape monopole antenna at 5.8 GHz is also demonstrated. Band stop property of EBG structure reduces surface waves, and therefore, the back lobe of a wearable antenna is reduced. The frequency detuning of antenna takes place due to high losses in human body. Suitably designed EBG structure reduces this undesirable effect and also improves front to back ratio. The proposed compact antenna with designed EBG has observed the impedance bandwidth of 5.60 GHz to 6.15 GHz which covers 5.8 GHz ISM band. Evaluation of antenna performance under bending condition and on-body condition is carried out. Effectiveness of EBG array structure for Specific Absorption Rate (SAR) reduction on three layer body model is demonstrated by simulations. Calculated values of SAR for tissue in 1 g and 10 g are both less than the limitations. In conclusion, it is appropriate to use the proposed antenna in wearable applications.

1. INTRODUCTION

A wearable antenna is an antenna that is specially designed to function while being worn on the body. These antennas can be integrated into clothing. Wearable antennas for in and on Body Area Networks (BAN) are designed by textile materials. It can communicate with other antennas on body surface or with an external antenna. These antennas are used in Wireless Body Area Networks (WBAN) for applications like health care, military, sports, etc. [1]. Due to such a wide application scope, in recent past new antenna topologies for wearable application including multiband, compact and wide band antennas have been rapidly evolving.

The general performance requirements for wearable antennas are low mutual influence between antenna and human body for high antenna efficiency, low SAR, small size, low profile, and Improved bandwidth [2]. Large bandwidth of textile antennas is needed as it makes them less sensitive to detuning arising from the adverse environmental influences. There are many methods to increase the bandwidth of textile antennas. SAR is a parameter used to evaluate power absorption in human tissue. Electromagnetic power absorbed by the body may pose potential health risks. Hence, the evaluation of SAR is also an important consideration in wearable antenna design. SAR should be well below standard acceptable limit. Many organizations including IEEE, ICNIRP, FCC have recommended limits

Received 6 July 2021, Accepted 24 September 2021, Scheduled 10 October 2021
* Corresponding author: Surendra Singh Rathod (surendra_rathod@spit.ac.in).
[1] Department of Electronics Engineering, Sardar Patel Institute of Technology, Andheri(W), Mumbai 400058, India. [2] Department of Electronics and Telecommunications Engineering, Padmabhushan Vasantdada Patil Pratisthan College of Engineering, Mumbai 400022, India.

on radiation emitted by these devices to protect public from overexposure to EM fields. According to the guidelines by FCC and ICNIRP, the SAR must be less than 2 W/kg averaged over 10 g and less than 1.6 W/kg averaged over 1 g of human tissue [3–5].

Some approaches that can be applied to improve the bandwidth as reported by various authors are briefly described below. Limitations and advantages of these approaches have to be considered in textile antenna designs: Increasing the substrate thickness of antenna increases its bandwidth. However, thick substrate configuration increases profile of the antenna. Low dielectric constant of textile material increases antenna bandwidth and reduces losses due to surface wave. However, this lowers radiation efficiency. Bandwidth can be improved by introducing parasitic elements. Feed networks in coplanar/stacked configuration are used. However, the feed network makes the antenna structure complicated and increases its size [6] Incorporation of slots in an antenna also improves its bandwidth. This approach also maintains a single-layer radiating structure to preserve the antenna's thin profile characteristic [7]. However, with this method, consistent broadside gain radiation patterns cannot be obtained throughout the matching bandwidth. Another limitation is that in order to maintain acceptable F/B ratio, a larger size ground plane has to be used. The ground plane makes a shield for human body, so the radiation does not transmit towards human body. It affects matching due to coupling. A high front to back ratio of radiation is desired to reduce this coupling. However, a large size ground plane results in the increase of the size which makes the design uncomfortable to the user. The presence of full ground plane results in a resonant semi-open cavity which narrows antenna bandwidth. Bandwidth can be improved by suitably designed EBG/AMC based antenna [8]. With uniplanar EBG increased bandwidth can be obtained in addition to adequate surface wave suppression [9].

Periodic arrangements of conductors and dielectric materials are commonly used to implement EBG structures. A properly designed EBG structure for an antenna provides many other advantages. The surface wave band gap property of EBG helps to increase gain, minimize backward wave radiation, and reduce SAR in human tissues. EBG surface limits the propagation of surface waves within a particular frequency band. Surface waves reduce the gain and efficiency of an antenna. EBG acts as an LC circuit and blocks propagation of surface waves, thus decreasing the level of undesired radiation towards the human body. Any EM wave in the stopband area is known to be reflected back by EBG structures. EBG plays a role of ground plane due to its in-phase reflection property.

When the antenna moves closer to human body, all the antenna parameters like resonant frequency, radiation pattern, bandwidth, and efficiency may change radically. Thus, it is difficult to miniaturize a wearable antenna while maintaining its high performance. When an antenna is used, it may be stretched and crumpled, causing deformation hence degrading its performance. In recent past, EBG/AMC based antenna designs have been reported to have better performance than other designs. An artificial magnetic structure (AMC) in combination with EBG is known to eliminate frequency detuning effect and thus improve radiator performance. Change in resonance frequency of antenna is termed as its frequency detuning. It is caused by bending (structural deformation), operation in close proximity of human body tissue, and moisture effects [10]. As human body has very high dielectric constant and wearable antenna is close to it, antenna frequency detunes [3]. EM coupling of human body to wearable antenna needs to be studied to asses the value of antenna frequency detuning. Reduction of EM coupling to human body should be studied as it may influence antenna performance frequency detuning and radiation degradation [11]. The EBG structure reduces SAR value, and it is widely used in wearable antenna design [12].

In recent years, several EBG structures have been investigated and reported for wearable textile antennas. Uniplanar compact and mushroom EBGs are the most common types of EBG configurations identified in the literature. Uniplanar compact EBG is most ideal for wearable applications due to no vias, low cost, compatibility with planar circuit technology, etc. In literature related to the design of EBG structures for wearable textile antenna the objective of robust, compact, low profile antenna design is accomplished by various methods [1, 3, 4, 13, 14]. In [1], a dual band coplanar patch antenna integrated with double concentric square EBG is designed. EBG unit cell patch size is $0.327\lambda_{c1}$, and it operates at 2.45 GHz and 5 GHz where λ_{c1} is the antenna operating frequency. This design reduces the radiations into the body as reported by authors. A fractal based dual band antenna integrated with a square slotted EBG with a unit cell size of $0.30\lambda_{c1}$ for wearable application is reported [3]. The antenna is backed with a 3×3 array of dimensions 150 mm $\times$ 150 mm. This design resulted into SAR reduction

and enhanced Front to Back Ratio (FBR). A dual band textile antenna loaded with artificial magnetic conductor plane of size 100 mm × 100 mm is proposed in [13] for wireless application. It is realized using flexible textile material, but vias affect the comfortness. A 3 × 3 rectangular ring shape array of unit cell size $0.216\lambda_{c1}$ of dimensions 81 mm × 81 mm is designed, and equivalent circuit model of EBG unit cells were investigated [14]. A compact wearable textile antenna using denim material integrated with 2 × 2 EBG array with unit cell size of $0.1\lambda_{c1}$ and overall dimension of 46 mm × 46 mm at 2.4 GHz for medical application [4] is investigated. However, these structures are too thick for Medical Body Area Network (MBAN) applications [1, 3, 13–17]. In [18, 19], authors use semi-flexible materials for wearable application. However, they are not sufficiently deformable and are uncomfortable for users, or suffer from low FBR [19–24]. A different approach in [25] uses a single-band multilayer wearable antenna EBG structure thus improving bandwidth. However, the fabrication of such a structure is complicated.

Most EBG designs reported in [1, 3, 13, 17–19, 21–24, 26, 27] have narrow bandwidth causing frequency shifts that are sensitive in the vicinity of the human body and during deformation [28]. In most of the reported literature, overall antenna size is large due to large periodic size of EBG structure. Reduction of textile antenna size is a challenge. This reduction has been attempted in this work as an original contribution. Apart from this, when textile antenna is used in wearable application, frequency detuning may take place due to human body loading and structure deformation effect. Larger antenna bandwidth is required to make it less sensitive to frequency detuning. In this work, bandwidth enhancement compared to reported wearable textile antennas [26, 29–31] is attempted.

Considering the above issues and requirements in this work, the design and analysis of a planar EBG structure with improved bandwidth is carried out. Section 2 presents a proposed EBG, its design and simulation results for refection phase, equivalent circuits, dispersion diagram, etc. Simulated transmission coefficient response using suspended microstrip line (SML) method is compared with measured results. Section 3 presents requirements of antenna from design perspective. Simulated and experimental results for reflection coefficient and radiation pattern for antenna with EBG are examined. The antenna integrated with designed EBG structure, reflection coefficient comparison (simulated and measured), and effect of antenna bending are described. In Section 4, simulations to asses the effect of EBG on SAR values using three layer body model are briefly described. The comparison of proposed structure with reported structures at 5.8 GHz is tabulated in terms of volume, bandwidth, and SAR values. Section 5 mentions conclusions drawn from this work.

2. PROPOSED EBG DESIGN, REFLECTION PHASE AND DISPERSION DIAGRAM

In this section, an EBG structure is modeled using Ansys HFSS simulation software which is useful for simulations of antenna structures. Useful outcomes from these simulations are reflection phase plot for assumed EBG unit cell dimensions.

2.1. EBG Unit Cell, Equivalent Circuit Model and Simulation Results

Dimensions of the EBG unit cell considered are shown in Figure 1. The operating frequency of 5.8 GHz is usually used in wireless local area network (WLAN) communication and wireless body area network (WBAN) [1, 32]. The choice of various dimensions in an EBG unit cell helps to achieve desired reflection phase at specified frequency. This EBG is to be used along with antenna at operating frequency, hence various dimensions of EBG are chosen accordingly. Here, a is the width of the outer slot, b the gap between inner square patch and outer slot, c the width of inner square patch, w the width of outer patch, u the length of outer patch, x the substrate width, and y the length of the substrate. Substrate material selected is denim. Parameters for the proposed EBG are taken as substrate dielectric constant $\epsilon_r = 1.7$, loss tangent = 0.02, substrate height $h = 0.7$ mm, height of inner square patch and outer slot = 0.17 mm, $w = 7$ mm, $u = 14$ mm, $a = 1$ mm, $b = 1$ mm, $c = 3$ mm, $x = 8$ mm, and $y = 15$ mm. The choice of these dimensions helped to achieve the specified/desired operating frequency as per equations in [33]. In order to implement EBG as a 2 × 2 array, 4 EBG unit cells are placed as shown in Figure 1. Here, g is the gap between two EBG cells. EBG unit cells are also analyzed using equivalent circuit model [14, 33–35]. Such a model gives equivalent L and C of a cell from which operating frequency may be determined. An approach similar to the one adapted in [36] was applied to the EBG unit cell shown in Figure 1.

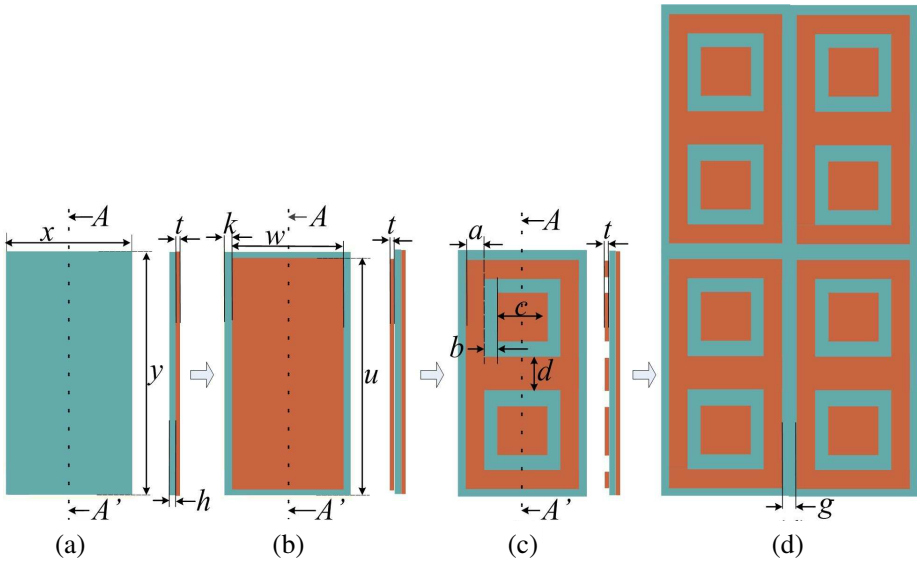

Figure 1. Evolution of EBG array, (a) EBG substrate, (b) outer patch, (c) inner patches, (d) 2×2 EBG array.

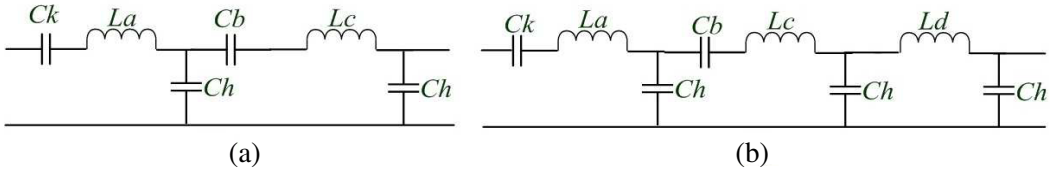

Figure 2. Equivalent circuit of EBG unit cell in (a) X direction, (b) Y direction.

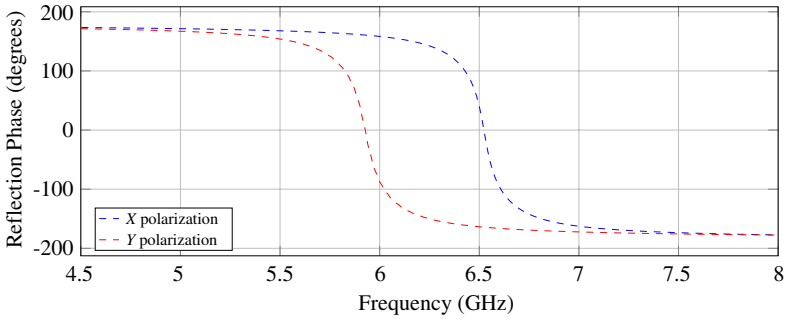

Figure 3. Simulated reflection phase response of proposed EBG unit cell.

The equivalent circuit obtained for EBG unit cell in X direction and Y direction is shown in Figure 2. Here, Ck, Cb are capacitance formed due to slots. Ch is the coupling capacitance between patch and substrate. La is the inductance due to outer slot while Lc is the inductance due to inner patch. From various dimensions of EBG structure, inductance and capacitance are calculated. Using Equations (1) and (2). Here, w is the width of each EBG patch.

$$L = \mu_0 h \tag{1}$$

$$C = \frac{w\epsilon_0(\epsilon_r + 1)}{\pi} \cosh^{-1}\frac{2w + g}{g} \tag{2}$$

EBG structure is analyzed in X polarization and Y polarization by two master/slave boundaries on the sides of unit cell. By deembedding the wave port impedance up to the top of cell, the phase of the

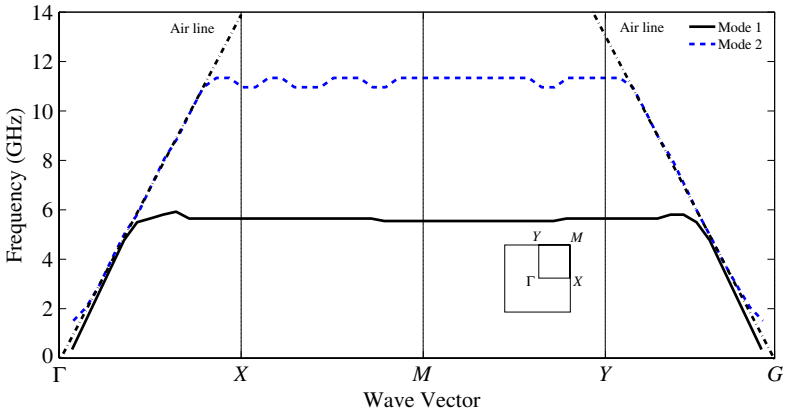

Figure 4. Dispersion diagram of the proposed EBG structure.

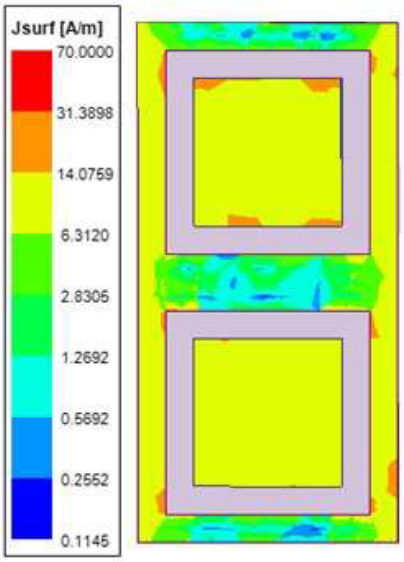

Figure 5. Simulation result of surface current distribution on EBG cell.

reflection coefficient is obtained. Figure 3 shows simulation result for reflection phase. It is observed from the figure that the proposed EBG structure reflects a normally incident wave with a 0 degree phase at frequencies shown in Figure 3. It shows perfect magnetic conductor (PMC) like characteristics whereas PMC characteristic is not observed in nature. EBG surface reflection phase varies from -180 degrees to $+180$ degrees with increasing frequency. Frequency region between $+90$ degrees and -90 degrees coincides with EBG.

The verification of a band gap property of a proposed EBG unit cell is carried out by the simulation of unit cell in Ansys HFSS [37]. The dispersion analysis of EBG unit cell is carried out with a rectangular symmetry (irreducible) Brillouin zone plot as shown in Figure 4. From the dispersion diagram shown in this figure, the band gap of 5.9–6.7 GHz in X direction and that of 5.64–6.3 GHz in Y direction are observed between mode 1 and mode 2 of the proposed EBG unit cell.

Figure 5 shows the surface current distribution obtained by simulations. It has been done on the metal layer of a unit cell from the EBG structure with a perpendicular incident electromagnetic wave. The incident wave frequency is 5.8 GHz, which is also the frequency point of zero reflection phase of the incident wave. It is observed from the figure that the surface current mainly concentrates on the outer slot. The distribution turns out to be symmetric about the vertical line across the central point. The current reaches the minimum at centers of upper side edge, middle edge, and down side

edges, and reaches the maximum at both centers of the left and right edges which forms the resonance characteristic of the first zero-phase point. The induced current also reaches maximum on both the inner square patches of EBG.

2.2. EBG Array, Simulation and Measured Results

From the EBG unit cell shown in Figure 1, a 5×5 array is formed. This array along with SML is simulated along Y direction [38]. Simulated S_{21} parameters are shown in Figure 6. In an SML structure, when current is supplied to the input transmission line, it performs charging and discharging of the current in the L and C components (Figure 2) from input transmission line till output transmission line. Within certain frequency range, where the LC circuit of the EBG has resonance, the current is looped regularly in the LC part of EBG structure and is suppressed from propagating [39]. Thus, transmission lines over EBG structures perform the band stop filter [3] operation. For frequencies within the band gap region, this structure blocks power transmitted along the strip line. This arrangement may be used to test transmission response of EM waves. SML with the entire EBG acts as a band reject filter at 5.94 GHz. Here, frequency range with attenuation losses of less than -10 dB is considered as the band gap. A 5×5 EBG array is made from copper tape (with dimensions as used in simulations) and is placed on a denim material with overall dimensions of $62 \times 97 \times 0.7\,\text{mm}^3$. Photographs of fabricated EBG with SML mounted in Y direction are shown in Figure 6. The distance between microstrip line and EBG surface is 1 mm with 0.2 mm air gap. Transmission coefficient S_{21} is measured by VNA. VNA used was Agilent technologies model no N9923A which can be used up to RF frequencies of 6 GHz. The measured S_{21} is found in close agreement with the simulated value.

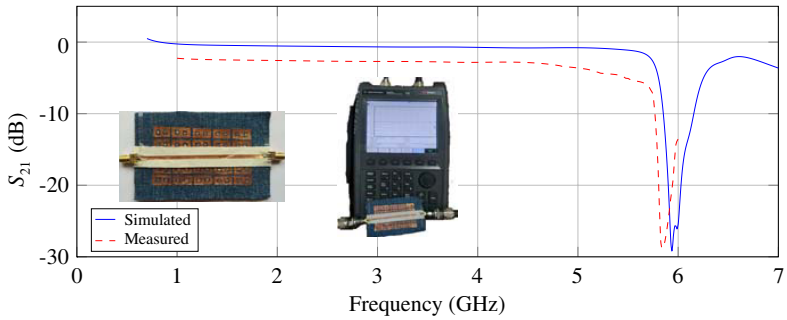

Figure 6. Comparison of simulated and measured EBG characteristics based on SML method.

3. APPLICATION OF PROPOSED EBG TO INVERSE E-SHAPE MONOPOLE ANTENNA

3.1. Inverse E-Shape Monopole Antenna Design

As mentioned in [40] a textile inverse E shaped microstrip monopole antenna is chosen to satisfy above mentioned desired features. However, this design needs to be modified for operating frequency of 5.8 GHz. As antenna is to be used in wearable application, a textile material needs to be used for substrate. Conducting material used is copper tape. The proposed textile inverse E shaped microstrip monopole antenna used has operating frequency of 5.8 GHz. The substrate used has length (L_1): 30 mm, width (w_1): 20 mm, material: denim, relative permittivity: $\epsilon_r = 1.7$, loss tangent: $\tan(\delta) = 0.02$, thickness (h) = 0.8 mm. The width of a 50 ohm microstrip feed line is 2.6 mm. Conducting sheet used is a copper tape with the thickness of 0.17 mm and conductivity of 5.8×10^7 S/m. Other parameters of inverse E shape microstrip monopole antenna are radiator patch length of 19.2 mm, radiator patch width of 12.2 mm, and ground plane length of 17.6 mm. With these specifications, the antenna is designed in Ansys HFSS. The model may be seen in Figure 7.

Figure 8 shows simulated and measured reflection coefficients of the fabricated antenna in free space. They are found in close agreement. S_{11} is found to be -14.39 dB at 5.87 GHz. The band range

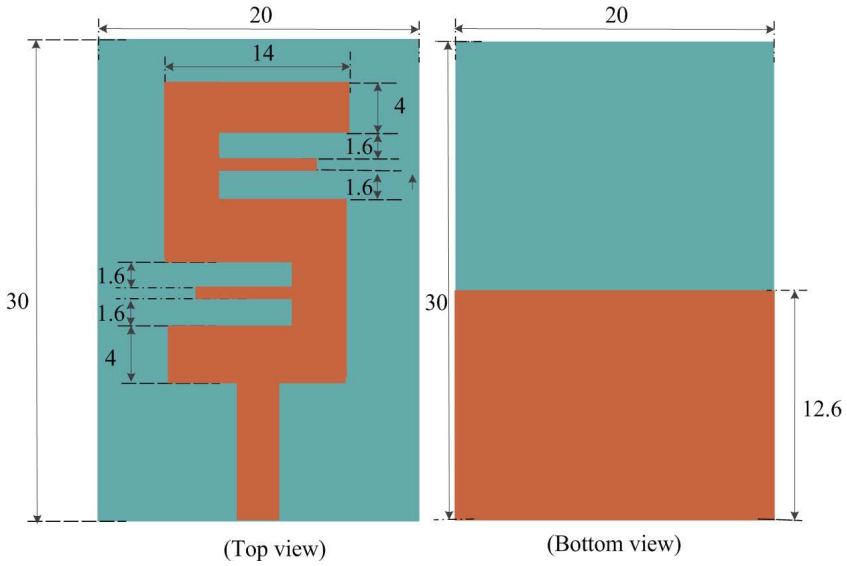

Figure 7. Inverse E-shaped monopole antenna configuration.

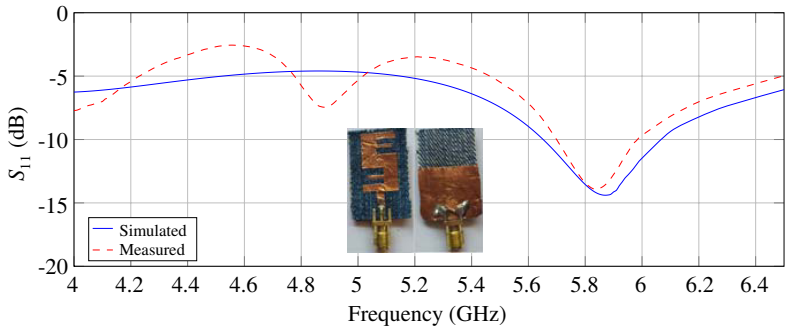

Figure 8. Comparison of simulated and measured S_{11} of antenna.

of the antenna is from 5.80 GHz to 6.05 GHz with bandwidth of 250 MHz. Simulated radiation patterns of the antenna in Y-Z plane (E-plane) and X-Z plane (H-plane) at the frequency of 5.94 GHz are shown in Figure 11. It is also observed that omnidirectional pattern in H plane and bidirectional in E plane are exhibited by the antenna. The radiation pattern in the E-plane exhibits maximum radiation in Z-direction whereas null appears in Y-direction.

3.2. Antenna with EBG

The antenna and EBG structure proposed above are placed together as shown in Figure 9. A 1-mm air gap spacing S1 is used in model. The simulated radiation patterns of the antenna in E and H planes with and without EBG are as shown in Figure 11. As seen in the figure, the unidirectional radiation patterns appear in both E and H planes. It is also observed that backward radiation decreases thus improving FBR by 20 dB. Figure 11 also shows experimentally measured radiation patterns in E and H planes obtained using the setup shown in Figure 10. The measured results are found in close agreement with simulated ones. The simulated reflection coefficient of the antenna with EBG in free space is as shown in Figure 12. The band range of the antenna with EBG is from 5.60 GHz to 6.15 GHz with the bandwidth of 550 MHz. Thus, it is concluded that the EBG structure enhances bandwidth from 250 MHz to 550 MHz. Figure 13 shows the comparison of simulated and measured reflection coefficients of the antenna with EBG. They are found in close agreement. The difference may be attributed to unavoidable errors in manual fabrication and assembly procedure for antenna and EBG.

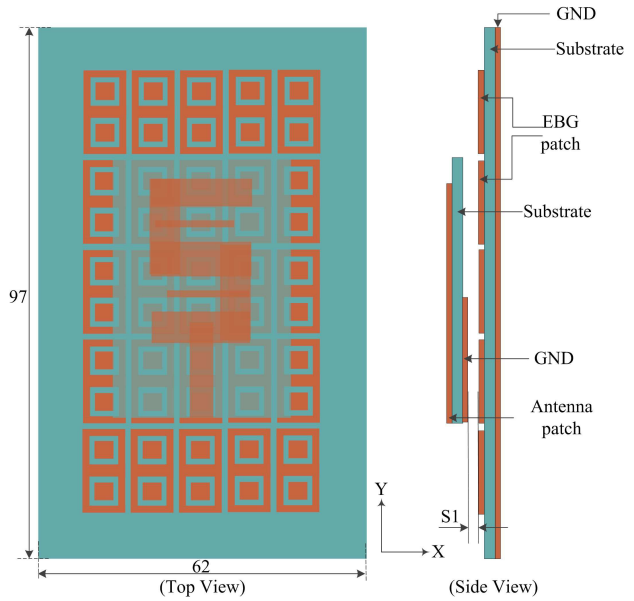

Figure 9. Inverse E-shape monopole antenna with EBG.

Figure 10. Experimental set up for radiation pattern measurement of antenna with EBG.

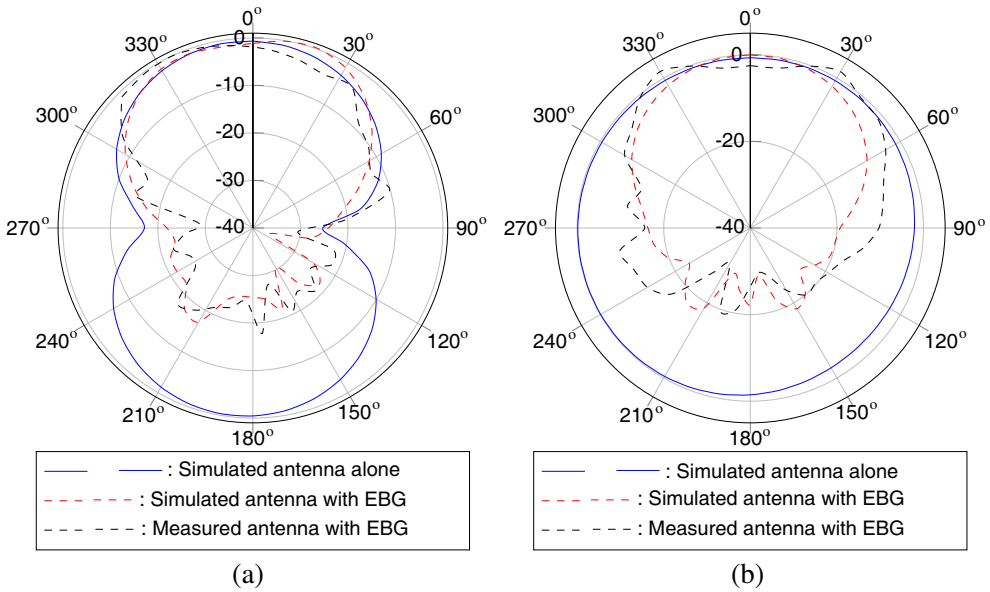

Figure 11. Simulated and measured radiation patterns of antenna in (a) E plane and (b) H plane.

3.3. Effect of Antenna Bending

To analyze the effect of bending experimentally, three foam cylinders with varying diameters were fabricated as shown in Figure 14. Diameters of the cylinder were 80 mm, 100 mm, and 120 mm which correspond to approximate human arm and leg diameters. The comparisons of measured reflection coefficient characteristics of antenna with EBG in free space with those on cylinders of different bending diameters in X and Y directions are shown in Figure 15. It is observed from Figure 15 that although the diameter of foam cylinder is varied, resonance frequency and operating frequency band are slightly shifted. The frequency of operation is sustained, and reflection coefficient S_{11} still maintains the bandwidth under bending condition.

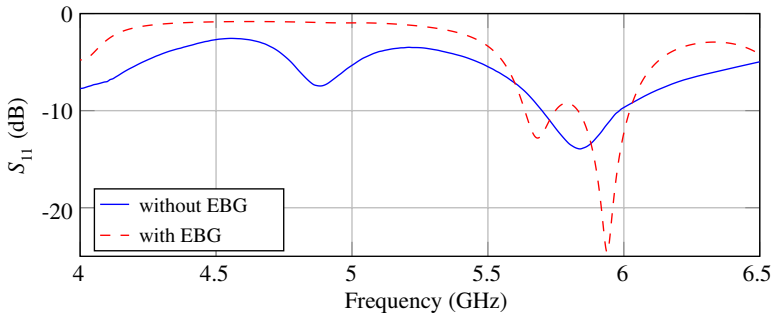

Figure 12. Comparison of simulated results of reflection coefficient of antenna with and without EBG.

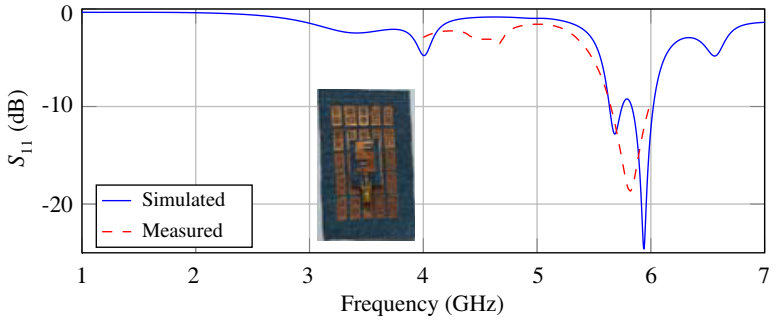

Figure 13. Comparison of simulated and measured reflection coefficient of antenna with EBG.

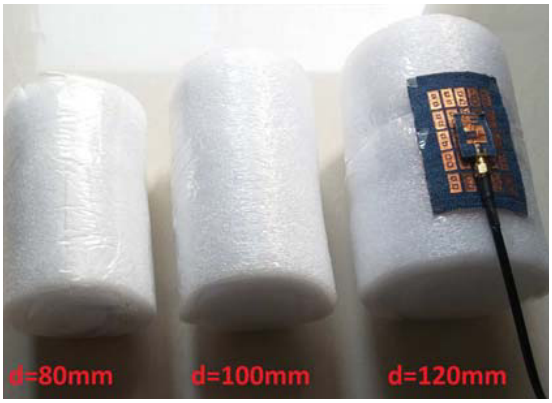

Figure 14. Fabricated foam cylinders of various diameters.

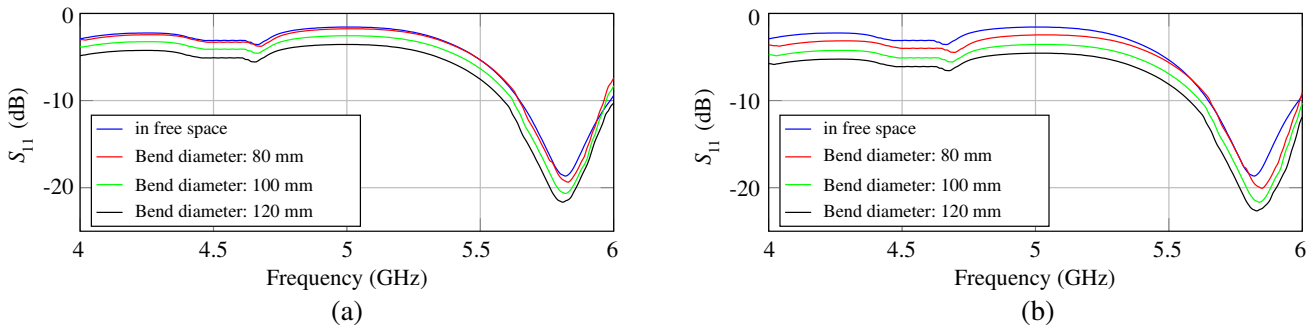

Figure 15. Comparison of measured S_{11} results of antenna with EBG in free space with measured results for different bending diameters in (a) X direction and (b) Y direction.

4. ANALYSIS OF SAR WITH PROPOSED EBG AND ANTENNA

When human body is exposed to EM field, a measure of energy absorption rate by a human body is termed as SAR [3]. The SAR level in human body due to antenna with and without EBG structure needs to be analyzed at design stage. This ensures that regulatory safety limits are obeyed. To analyze the SAR level in human body due to wearable antenna without and with EBG structure, a three layer human rectangular body model is used. It consists of three layers representing skin, fat, and muscle. Properties and dimensions of various layers are as mentioned in Table 1 [41]. The input power applied to the antenna to calculate SAR is selected as 1 W (rms). The separation of antenna with EBG from skin in model is assumed as 1 mm. The calculation of SAR is based on the IEEE C95.1 standard prototype provided in Ansys HFSS. SAR values computed on three layer body model with only antenna are shown in Figure 16(a). It is computed to be in range of 0 to 25 W/Kg. Figure 16(b) shows computed SAR values in body model when the antenna along with EBG is incorporated. Table 2 shows the comparison of SAR values of the antenna with and without EBG structure over 1 g and 10 g tissue. It is observed that averaged values are lower for the antenna with EBG structure than those without EBG, thus showing the effectiveness of EBG. SAR values of the antenna with EBG structure obey the required limits as mentioned in various standards. Great disparity of SAR values between the case of only antenna and case of antenna with EBG has strongly proved that the adoption of an EBG structure has the effect of reducing the SAR values drastically. The antenna with EBG was tested in free space and on body for S_{11}. Comparison is shown in Figure 17. Results are found in close agreement. Table 3 shows the comparison of proposed EBG structure with those reported in literature at 5.8 GHz. The comparison is carried out in terms of volume, bandwidth, and SAR values. It is concluded from Table 3 that the antenna integrated with proposed EBG structure has small volume compared to other reported structures. Bandwidth improvement has been obtained as compared to those reported in [26, 29–31].

Table 1. Properties of various layers in multilayer human model.

Layer	Thickness mm	ϵ_r	Conductivity σ (S/m)	Density kg/m^3
Skin	2	35	3.8	1001
Fat	5	4.95	0.3	900
Muscle	20	48.4	5.12	1006

Table 2. SAR values with and without EBG.

Averaged value	SAR without EBG (W/kg)	SAR with EBG (W/kg)
1 g	25	0.6
10 g	10.12	0.056

Table 3. Comparison of proposed structure with exiting structures at 5.8 GHz.

Ref.	Volume (mm^3)	Bandwidth (%)	SAR (W/kg)
[29]	$0.77\lambda_0 \times 0.77\lambda_0 \times 0.135\lambda_0$	6.35	0.1 (1 g), 0.271 (10 g)
[30]	$1.45\lambda_0 \times 1.45\lambda_0 \times 0.019\lambda_0$	3.96	NA
[26]	$\pi \times (0.97\lambda_0)^2 \times 0.05\lambda_0$	8.10	0.312 (1 g), 1.21 (10 g)
[31]	$0.79\lambda_0 \times 0.92\lambda_0 \times 0.019\lambda_0$	4.83	1.5 (1 g), NA
P.W.	$1.19\lambda_0 \times 1.77\lambda_0 \times 0.04\lambda_0$	9.48	0.6 (1 g), 0.056 (10 g)

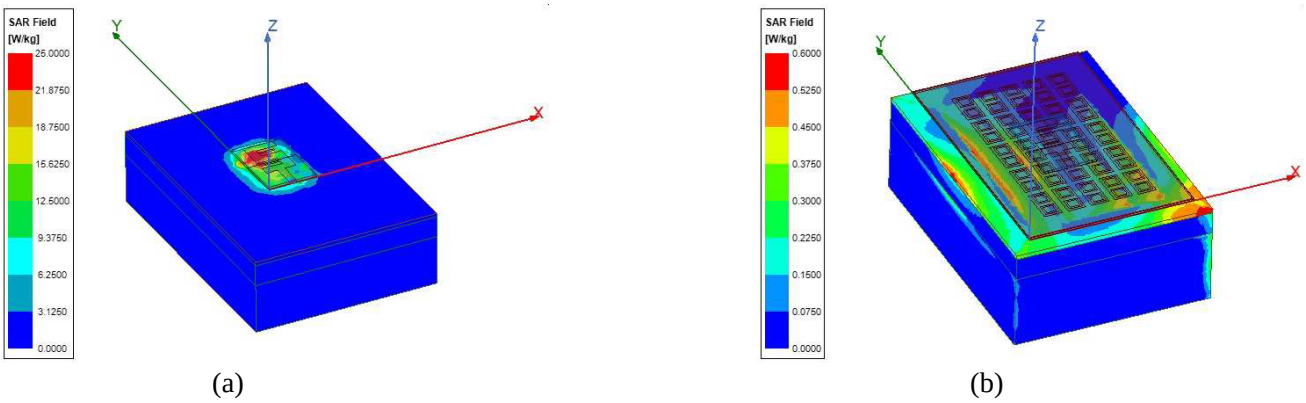

Figure 16. Simulated SAR values in three layer body model without EBG and with EBG, (a) without EBG, (b) with EBG.

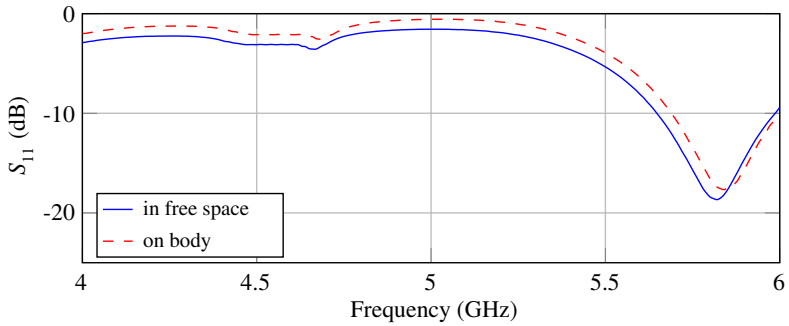

Figure 17. Comparison of measured reflection coefficient of antenna with EBG in free space and on body.

5. CONCLUSION

Design, analysis, simulations, and important experimental measurement of a rectangular eight shaped EBG structure has been attempted in this work. Antenna design at 5.8 GHz has been carried out in HFSS, and the proposed EBG structure is integrated with it. Experimental measurements related to antenna with and without EBG have been found in close agreement with designed values. Measured S_{11} shows that the antenna with EBG has good impedance matching at 5.8 GHz in the ISM band. Designed EBG with antenna has smaller volume and wider bandwidth than those already reported in literature. Besides, bending analysis and on-body measurements have been done, and it is observed that results are stable. The antenna has been placed on a three layer body model, and SAR values have been studied without and with an EBG structure. SAR in body model with the proposed EBG structure is acceptable as per international standards. Hence, the proposed EBG structure forms a suitable candidate for wearable applications.

REFERENCES

1. Zhu, S. and R. Langley, "Dual-band wearable textile antenna on an EBG substrate," *IEEE Trans. Antennas Propag.*, Vol. 57, No. 4, 926–935, Apr. 2009.
2. Haga, N., K. Saito, M. Takahashi, and K. Ito, "Characteristics of cavity slot antenna for body-area networks," *IEEE Trans. Antennas Propag.*, Vol. 57, No. 4, 837–843, 2009.
3. Velan, S., et al., "Dual-band EBG integrated monopole antenna deploying fractal geometry for wearable applications," *IEEE Antennas Wireless Propag. Lett.*, Vol. 14, 249–252, 2015.

4. Ashyap, Y. I., et al., "Compact and low-profile textile EBG-based antenna for wearable medical applications," *IEEE Antennas and Propagation Magazine*, Vol. 16, No. 1, 2550–2553, 2017.
5. Guido, K. and A. Kiourti, "Wireless wearables and implants: A dosimetry review," *Bioelectromagnetics*, Vol. 41, 3–20, 2020.
6. Pinapati, S. P., J. Brittain, A. Caldow, and C. Fumeaux, "Wearable textile EBG-inspired bandwidth-enhanced patch antenna," *IET Microwaves, Antennas and Propagation*, Vol. 14, No. 15, 2011–2019, 2020.
7. Meng, F., L. Ying, and S. K. Sharma, "A miniaturized patch antenna with enhanced bandwidth by using reactive impedance surface ground and coplanar parasitic patches," *Int. J. RF Microw. Comput. Aided Eng.*, Vol. 30, e22225, 2020, https://doi.org/10.1002/mmce.22225.
8. Cos, M. E., Y. Alvarez, and F. Las-Heras, "Enhancing patch antenna bandwidth by means of uniplanar EBG-AMC," *Microw. Opt. Technol. Lett.*, Vol. 53, 1372–1377, 2011.
9. Ashyap, A. Y. I., et al., "An overview of electromagnetic band-gap integrated wearable antennas," *IEEE Access*, Vol. 8, 7641–7658, Jan. 2020, doi: 10.1109/ACCESS.2020.2963997.
10. Pinapati, S. P., S. J. Chen, D. Ranasinghe, and C. Fumeaux, "Detuning effects of wearable patch antennas," *2017 IEEE Asia Pacific Microwave Conference (APMC)*, 162–165, 2017, doi: 10.1109/APMC.2017.8251403.
11. Alemaryeen, A. and S. Noghanian, "On-body low-profile textile antenna with artificial magnetic conductor," *IEEE Trans. Antennas. Propag.*, Vol. 67, No. 6, 3649–3656, Jun. 2019, doi: 10.1109/TAP.2019.2902632.
12. Sugumaran, B., R. Balasubramanian, and S. K. Palaniswamy, "Reduced specific absorption rate compact flexible monopole antenna system for smart wearable wireless communications," *Journal of Engineering Science and Technology*, Vol. 24, No. 3, 682–693, Jun. 2021.
13. Yan, S., P. J. Soh, and G. A. E. Vandenbosch, "Low profile dual band textile antenna with artificial magnetic conductor plane," *IEEE Trans. Antennas. Propag.*, Vol. 61, No. 12, 6487–6490, Dec. 2014.
14. Gao, G.-P., B. Hu, S.-F. Wang, and C. Yang, "Wearable circular ring slot antenna with EBG structure for wireless body area network," *IEEE Antennas Wireless Propag. Lett.*, Vol. 17, No. 3, 434–437, Mar. 2018.
15. Gao, G., R. Zhang, C. Yang, H. Meng, W. Geng, and B. Hu, "Microstrip monopole antenna with a novel UC-EBG for 2.4 GHz WBAN applications," *IET Microwaves, Antennas and Propagation*, Vol. 13, No. 13, 2319–2323, Oct. 2019.
16. Gao, G., S. Wang, R. Zhang, C. Yang, and B. Hu, "Flexible EBG-backed PIFA based on conductive textile and PDMS for wearable applications," *Microw. Opt. Technol. Lett.*, Vol. 62, No. 4, 1733–1741, 2020.
17. Kamardin, K., et al., "Planar textile antennas with artificial magnetic conductor for body-centric communications," *Appl. Phys. A Mater. Sci. Process.*, Vol. 4, No. 4, 1–9, 2016.
18. Jiang, Z., D. E. Brocker, P. E. Sieber, and D. H. Werner, "A compact, low-profile metasurface-enabled antenna for wearable medical body area network devices," *IEEE Trans. Antennas Propag.*, Vol. 62, No. 8, 4021–4030, Aug. 2013.
19. Abbasi, M. A. B., S. S. Nikolaou, M. A. Antoniades, M. Nikolic Stevanovic, and P. Vryonides, "Compact EBG-backed planar monopole for BAN wearable applications," *IEEE Trans. Antennas Propag.*, Vol. 65, No. 2, 453–463, Feb. 2017.
20. Raad, H. R., A. I. Abbosh, H. M. Al-Rizzo, and D. G. Rucker, "Flexible and compact AMC based antenna for telemedicine applications," *IEEE Trans. Antennas Propag.*, Vol. 61, No. 2, 524–531, Feb. 2013.
21. Agarwal, K., Y.-X. Guo, and B. Salam, "Wearable AMC backed nearend re antenna for on-body communications on latex substrate," *IEEE Trans. Compon., Packag., Manuf. Technol.*, Vol. 6, No. 3, 346–358, Mar. 2016.
22. Jiang, Z. H., Z. Cui, T. Yue, Y. Zhu, and D. H. Werner, "Compact, highly efficient, and fully flexible circularly polarized antenna enabled by silver nanowires for wireless body-area networks," *IEEE Trans. Biomed. Circuits Syst.*, Vol. 11, No. 4, 920–932, Aug. 2017.

23. Ashyap, A. Y. I., et al., "Highly efficient wearable CPW antenna enabled by EBGFSS structure for medical body area network applications," *IEEE Access*, Vol. 6, 77529–77541, 2018.
24. Ashyap, A. Y. I., Z. Zainal Abidin, S. H. Dahlan, H. A. Majid, and G. Saleh, "Metamaterial inspired fabric antenna for wearable applications," *Int. J. RF Microw. Comput.-Aided Eng.*, Vol. 29, No. 3, Mar. 2019.
25. Mustafa, A. B. and T. Rajendran, "Wearable multilayer patch antenna with electromagnetic band gap structure for public safety systems," *IETE Journal of Research*, 1–10, 2020, doi: 10.1080/03772063.2020.1739572.
26. Jinpil, T., H. Youngtaek, and C. Jaehoon, "Textile antenna with EBG structure for body surface wave enhancement," *Electronics Letters*, Vol. 51, No. 15, 1131–1132, 2015.
27. Ashyap, A. Y. I., et al., "Flexible antenna with HIS based on PDMS substrate for WBAN applications," *Proc. IEEE Int. RF Microw. Conf. (RFM)*, 69–72, Dec. 2018.
28. Ashyap, A. Y. I., et al., "Robust and efficient integrated antenna with EBG-DGS enabled wide bandwidth for wearable medical device applications," *IEEE Access*, Vol. 8, 56346–56358, 2020, doi: 10.1109/ACCESS.2020.2981867.
29. Bjorninen, T. and F. Yang, "Low-profile head-worn antenna with a monopole-like radiation pattern," *IEEE Antennas Wireless Propag. Lett.*, 14, 2015.
30. Hong, Y., T. Jinpil, and C. Jaehoon, "An all textile SIW cavity-backed circular ring slot antenna for WBAN applications," *IEEE Antennas Wireless Propag. Lett.*, 15, 2016.
31. Kang, D.-G., T. Jinpil, and C. Jaehoon, "Low-profile dipole antenna with parasitic elements for WBAN applications," *Microw. Opt. Technol. Lett.*, Vol. 58, 1093–1097, 2015.
32. Gao, G., B. Hu, S. Wang, and C. Yang, "Wearable planar inverted-F antenna with stable characteristic and low specific absorption rate," *Microw. Opt. Technol. Lett.*, Vol. 60, No. 4, 876–882, Apr. 2018.
33. Sievenpiper, D., L.-J. Zhang, R. Broas, N. G. Alexopolous, and E. Yablonovitch, "High-impedance electromagnetic surfaces with a forbidden frequency band," *IEEE Trans. Microw. Theory Tech.*, Vol. 47, No. 11, 2059–2074, Nov. 1999.
34. Bhavarthe, P. P., S. S. Rathod, and K. T. V. Reddy, "A compact dual band gap electromagnetic band gap structure," *IEEE Trans. Antennas Propag.*, Vol. 67, No. 1, 596–600, Jan. 2019.
35. Bhavarthe, P. P., S. Rathod, and K. Reddy, "A compact two via slot type electromagnetic-bandgap structure," *IEEE Microwave and Wireless Components Letters*, Vol. 27, No. 5, 446–448, May 2017.
36. Lamminen, A. E. I., A. R. Vimpari, and J. Saily, "UC-EBG on LTCC for 60-GHz frequency band antenna applications," *IEEE Antennas Wireless Propag. Lett.*, Vol. 57, No. 10, 2904–2912, Oct. 2009.
37. Remski, R., "Analysis of photonic bandgap surfaces using ansoft HFSS," *Microwave Journal*, Vol. 43, No. 9, 190–199, Sept. 2000.
38. Yang, L., M. Fan, F. Chen, J. She, and Z. Feng, "A novel compact electromagnetic-bandgap (EBG) structure and its application for microwave circuits," *IEEE Trans. Microw. Theory Tech.*, Vol. 53, No. 1, 183–190, Jan. 2005.
39. Ayop, O. and M. K. A Rahim, "Analysis of mushroom-like electromagnetic band gap structure using suspended transmission line technique," *2011 IEEE International RF and Microwave Conference*, 258–261, 2011, doi: 10.1109/RFM.2011.6168743.
40. Ashyap, A. Y. I., et al., "Inverted E-shaped wearable textile antenna for medical applications," *IEEE Access)*, 6, 2018.
41. Sakthi, B. and S. Esther, "EBG backed flexible printed Yagi-Uda antenna for on-body communication," *IEEE Access*, 5, 2017.